A Robust Nonlinear Scale Space Change Detection Approach for SAR Images

Berk Sevilmis[a], O. Erman Okman[a], Fatih Nar[a], Can Demirkesen[a], and Mujdat Cetin[b]

[a]SDT Space and Defence Technologies, Galyum Blok No:2 ODTU Teknokent Ankara, Turkey
[b]Faculty of Engineering and Natural Sciences, Sabanci University, Istanbul, Turkey

ABSTRACT

In this paper, we propose a change detection approach based on nonlinear scale space analysis of change images for robust detection of various changes incurred by natural phenomena and/or human activities in Synthetic Aperture Radar (SAR) images using Maximally Stable Extremal Regions (MSERs). To achieve this, a variant of the log-ratio image of multitemporal images is calculated which is followed by Feature Preserving Despeckling (FPD) to generate nonlinear scale space images exhibiting different trade-offs in terms of speckle reduction and shape detail preservation. MSERs of each scale space image are found and then combined through a decision level fusion strategy, namely *"selective scale fusion"* (SSF), where contrast and boundary curvature of each MSER are considered. The performance of the proposed method is evaluated using real multitemporal high resolution TerraSAR-X images and synthetically generated multitemporal images composed of shapes with several orientations, sizes, and backscatter amplitude levels representing a variety of possible signatures of change. One of the main outcomes of this approach is that different objects having different sizes and levels of contrast with their surroundings appear as stable regions at different scale space images thus the fusion of results from scale space images yields a good overall performance.

Keywords: Change detection, multitemporal SAR images, log-ratio image, scale space representation, MSER, fusion.

1. INTRODUCTION

With the advent of improved sensing technologies in spaceborne and airborne systems, multitemporal remote sensing images have been actively utilized to infer dynamics of regions being monitored. Change detection analysis has been one of the key concepts aiding several disciplines such as environmental monitoring and urban planning. The goal of change detection is to identify any physical changes in the scene such as natural disasters, land cover change, flood, etc. as well as changes in man-made structures and in location of objects including movement, appearance and disappearance between the image acquisition times. Even if the interest of change is constrained to a specific event, the same kind of event can have different signatures depending on where it takes place and on the characteristics of the sensor.[1] Thus an ideal change detection algorithm should be void of false detections that can be induced by SAR artifacts such as side-lobes, moving reflectors and/or inherent sensor noise, speckle, radar illumination, incidence or aspect angle changes.[2] In order to carry out meaningful data analysis and hence perform change detection, most often preprocessing steps are adopted including speckle reduction, sensor calibration, radiometric calibration and geometric registration of multitemporal images to circumvent the effects of the abovementioned artifacts to some extent.

In the literature, within a binary classification rationale, several unsupervised change detection algorithms are brought forward aiming to spot regions of change in multitemporal images in the absence of any accompanying prior information to model classes. For instance, Mercier *et al.*[3] presented a methodology quantifying the probability density function evolution of the multitemporal SAR images between the acquisition times to spot abrupt ground changes in which the backscatter returns of temporal images are modeled with Gaussian mixtures. Bazi *et al.*[4] proposed a feedback driven unsupervised change detection scheme based on Kittler-Illingworth (KI) thresholding technique applied on the generalized Gaussian distribution used to model the changed and unchanged classes. The method achieves automatic change detection through minimizing a modified KI criterion cost by exploiting a pre-defined set of filtering iterations on multitemporal SAR images. Moser *et al.*[5] extended the KI minimum-error thresholding algorithm by modeling SAR amplitude data with Nakagami-Gamma, Weibull

Image and Signal Processing for Remote Sensing XIX, edited by Lorenzo Bruzzone,
Proc. of SPIE Vol. 8892, 889215 · © 2013 SPIE · CCC code: 0277-786X/13/$18
doi: 10.1117/12.2030189

and log-normal probability density distributions. The approach attains promising results besides automating the threshold selection procedure by minimizing the generalized Kittler and Illingworth (GKIT) criterion cost provided that the ratio image is adequately filtered where the adaptive Gamma-MAP filter is used to reduce speckle noise. The selection of the number of filtering iterations remains empirical and an extensive analysis of optimum filtering iterations is not performed. In all the preceding techniques, the pixel backscatter amplitudes are assumed independent identically distributed random variables forming a process where no spatial correlation is exploited. Within a statistical perspective, context independent unimodal statistical fitting becomes inappropriate where sea surface, different ice types, extremely heterogeneous clutter such as urban regions, bare ground surfaces are mostly known to follow Weibull, modified beta, G^0, and normal distributions respectively.[6] Huang *et al.*[7] developed a local texture analysis based change detection algorithm making use of various spatial texture features calculated from Gray-level Cooccurrence Matrix (GLCM) of temporal images. Next, decision level fusion is performed by aggregating and majority voting the decisions of each feature specific change maps obtained by virtue of the EM algorithm. Zhang *et al.*[8] utilized probabilistic patch-based filter (PPB) along with graph-cut segmentation algorithm to reduce speckle noise and to initialize the change map prior. The initial change mask is then used to aid MAP estimation assuming the difference image follows a generalized Gaussian distribution (GGD). Though the graph-cut algorithm provides spatial prior information, this information is not fully utilized in the subsequent MAP estimation and each pixel is independently classified using ratio of posterior probabilities which involves experimental threshold selection. Celik *et al.*[9] proposed the use of the genetic algorithm to obtain a change detection mask without explicitly computing a difference image. A multiobjective cost function is defined to sort out chromosomes used to breed in the next generation where both crossover and mutation operators are exploited. The method performs well for a wide range of change detection applications but suffers innate computational cost of genetic algorithms. Yetgin[10] adopted k-means clustering of the feature space consisting of vectors that are obtained by block partitioning the log-ratio image and properly modified via Local Gradual Descent Matrix (LGDM) to introduce local contextual information. The qualitative and quantitative results of the algorithm demonstrate that it performs well in detecting the boundaries of changes accurately. To incorporate spatial contextual information, Moser *et al.*[11] suggested Markovian data fusion on multichannel ratio image obtained from multichannel SAR amplitude images utilizing the GKIT technique to set the hypothesis prior for each pixel. The fusion is then accomplished within an energy function where parameter estimations are carried out using the Landgrebe and Jackson Expectation Maximization (LJ-EM) algorithm. Though the joint multivariate probability density function of channels are not elaborated upon, weighting of marginal probability density functions are considered going beyond a naive independence assumption thus in turn generating accurate change map.

Recently, transform domain methods and multiscale analysis steered the research predicating on the idea that different compromises on speckle reduction and shape detail preservation help obtain an enriched set of representation. To exemplify, Inglada *et al.*[1] introduced a local similarity measure between multitemporal images, namely Kullback-Leibler distance between probability density functions approximated by Edgeworth series expansion, aimed to obtain a change map indicating a confidence level of change at each pixel. The selection of different window sizes inherent to local statistics estimation is made use of generating a multiscale representation enabling fusion of scales, yielding a better performance than a monoscale detector. Bovolo *et al.*[12] introduced a multiscale driven change detection approach by applying wavelet decomposition to the log-ratio image and analyzing local coefficient of variation at each pixel to help determine its set of reliable scales. An independent set of threshold values, determined either automatically or manually, is used to binarize the scale images and several fusion methodologies mapping correspondences between reliable scale sets and binarized scale images are studied. The approach acquires good performance only to be affected by the thresholding process adopted. Bazi *et al.*[13] employed a series of scalar Mumford-Shah segmentations on multiresolution representation of the difference image by starting from the coarsest resolution image and treating the prior segmentation result as the initiation for the succeeding finer resolution image based on the idea that each segmentation result needs only be upsampled by a factor of two. The change map is then obtained when the finest resolution image is segmented. Celik[14] proposed a multiscale representation of the log-ratio image using the Undecimated Discrete Wavelet Transform (UDWT) coupled with k-means clustering on multiscale feature vectors extracted by sampling of neighborhood data at each pixel thereby obtaining intra-scale feature vectors aspiring to incorporate spatial contextual information. The proposed algorithm is shown to be robust to speckle noise realizing superior

performance compared to EM-based and MRF-based methods. Celik *et al.*[15] offered a multiresolution image analysis motivated unsupervised change detection method where UDWT is exploited providing different representations of the ratio image in terms of resolution, hence constituting a feature vector at each pixel. The scalar Chan-Vese active contour model segmentation is extended to vector-valued images and the evolved contour upon convergence of the algorithm designates the outer boundary of the regions forming the change map. The effect of the number of multiresolution levels on algorithm performance is carried out but the investigation of the optimum set of levels is not fully considered.

To evaluate the main trends in the literature, in general, the performance of thresholding based methods suffer from inadequate statistical model selection, specifically when the scene at hand is comprised of different clutter types, and is highly affected by the parameter estimation technique used. Lack of spatial contextual information results in construction of changed areas having discontinuous and inaccurate boundaries. On the other hand, though MRF-based methods take spatial dependency of backscatter amplitudes into consideration, they are generally computationally demanding. Segmentation- based approaches intend to properly recover object boundaries, built on some spatial similarity metric, and have been integrated within change detection algorithms recently.

In this paper we propose a segmentation-coupled change detection approach by making use of Maximally Stable Extremal Region (MSER)[16] analysis on multiscale images obtained by Feature Preserving Despeckling (FPD)[17] applied on log-ratio image owing to the fact that the changed areas are in contrast with their surroundings due to backscatter amplitude increase or decrease between image acquisition times. The advantage of applying FPD is twofold. Firstly, it helps reduce speckle noise thus reconstructs images composed of homogeneous regions in terms of texture. Secondly, utilizing different parameter choices, and hence exploring different trade-offs between speckle reduction and detail preservation through FPD, leads to the construction of a nonlinear scale space where boundaries of objects are better kept. The MSER analysis of scale space images yields that highly changed regions having a high contrast signature in the log-ratio image are properly segmented provided that an adequate amount of speckle reduction is achieved. Meanwhile, depending on the parameters of the FPD operator, this speckle reduction can result in a complete diffusion of slightly changed regions having relatively lower contrast signature in the log-ratio image into background clutter hampering their segmentation. Taking advantage of a decision level fusion strategy of MSERs obtained from each scale space image helps prevent possible misdetections achieving promising change detection results both on synthetically generated and real multitemporal SAR images and forms the main motive of the paper.

The paper is organized as follows. Section 2 describes and elaborates on the proposed change detection algorithm. Section 3 introduces the data sets and the experimental analysis and finally Section 4 concludes the paper giving insights for potential future work.

2. THE PROPOSED CHANGE DETECTION ALGORITHM

Let us assume that two geometrically registered SAR amplitude images are obtained where a radiometrically indifferent acqusition process is employed and let $I_{t_1} : [0, H[\cap\mathbb{N}\times[0, W[\cap\mathbb{N} \to \mathbb{R}$, $I_{t_2} : [0, H[\cap\mathbb{N}\times[0, W[\cap\mathbb{N} \to \mathbb{R}$ denote the multitemporal images of size $H \times W$ pixels, acquired on the same geographical area but at different times, t_1 and t_2, respectively. The purpose of the change detection algorithm is to map the domain of the image, on which the multitemporal images are defined, to a binary set where any changes in the natural environment or in man-made structures are differentiated. Hence the output of the algorithm, generally called the change map, can be represented as $I_{CM} : [0, H[\cap \mathbb{N} \times [0, W[\cap \mathbb{N} \to \{0, 1\}$.

Our proposed change detection method is comprised of four stages (as depicted in Fig. 1):

1) generation of the log-ratio image,

2) creating a nonlinear scale space by virtue of FPD,

3) MSER extraction of scale space images, and

4) change map generation through fusion using the proposed – selective scale fusion (SSF) method.

These steps are detailed in the subsequent subsections.

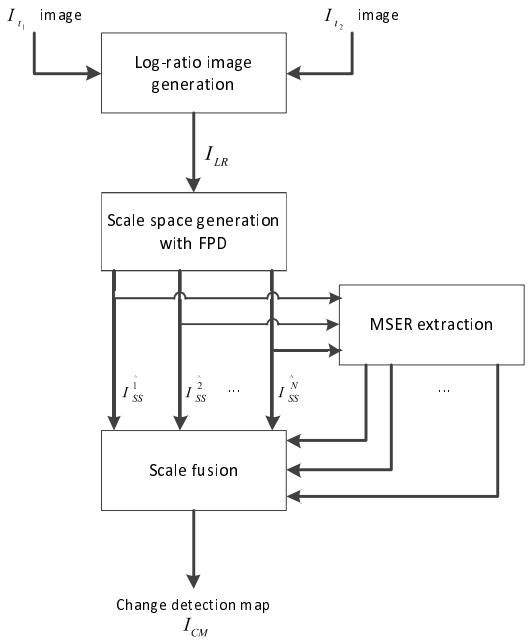

Figure 1: Overview of the proposed change detection algorithm.

2.1 Generation of the log-ratio image

The first step of the proposed algorithm is to generate the log-ratio image. As rationing is able to identify relative backscatter amplitude change between image acquisition dates irrespective of the level of backscatter amplitude difference and due to the ever-decreasing slope of the logarithm function between zero and one, log-ratio method is generally opt for SAR imagery to provide contrast stretching. Let I_{LR} denote the log-ratio image, we propose to slightly modify the log-ratio operator in order to handle the cases of objects entering and departing the scene between image acquisition times. These cases are associated with backscatter amplitude increase or decrease at a given pixel. In this way, we eliminate the need of a two-pass change detection algorithm. In particular, we define the log-ratio image as follows:

$$I_{LR} = 1 - \min\left\{\log\left(1 + \frac{I_{t_1}}{I_{t_2}}\right), \log\left(1 + \frac{I_{t_2}}{I_{t_1}}\right)\right\}. \tag{1}$$

2.2 Nonlinear scale space creation

Cetin *et al.*[17] formulated the SAR image reconstruction from complex-valued data problem as an optimization problem with a cost functional consisting of data fidelity and prior information. We propose to use a special case of this approach on the real valued log-ratio image to obtain its several different reconstructions, constituting the scale space representation $\mathbf{I}_{SS}$, i.e.,

$$\mathbf{I}_{SS} = \left\{I_{SS}^{\hat{1}},\, I_{SS}^{\hat{2}}, ...,\, I_{SS}^{\hat{N}}\right\}$$

$$I_{SS}^{\hat{n}} = \arg\min_{I_{SS}^{n}} J\left(I_{SS}^{n}\right)$$

$$J\left(I_{SS}^{n}\right) = \left\|I_{LR} - I_{SS}^{n}\right\|_2^2 + \left(\lambda_1^n\right)^2 \left\|I_{SS}^{n}\right\|_k^k + \left(\lambda_2^n\right)^2 \left\|DI_{SS}^{n}\right\|_k^k \tag{2}$$

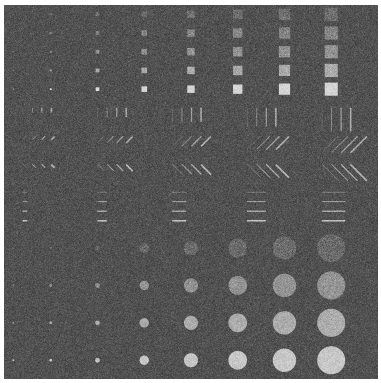

(a) Log-ratio image.

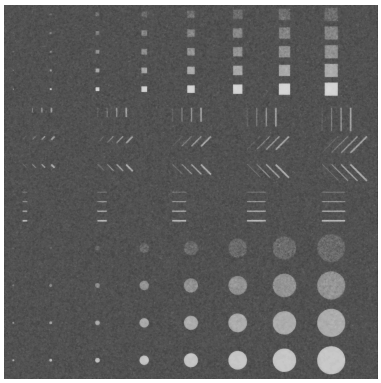

(b) $I_{SS}^{\hat{1}}$ with $\lambda_1^1 = 0$ and $\lambda_2^1 = 15$.

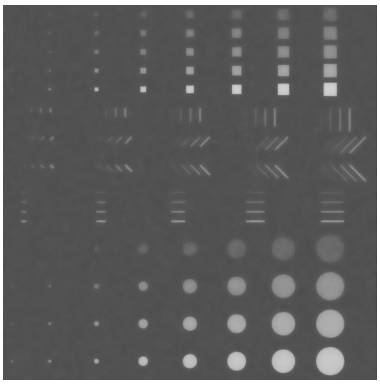

(c) $I_{SS}^{\hat{2}}$ with $\lambda_1^2 = 0$ and $\lambda_2^2 = 30$.

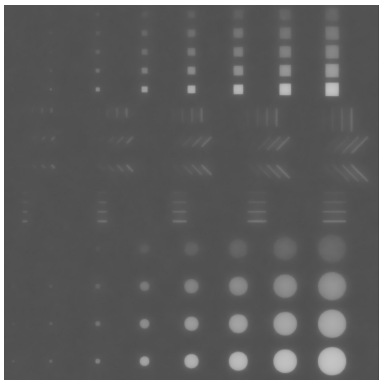

(d) $I_{SS}^{\hat{3}}$ with $\lambda_1^3 = 0$ and $\lambda_2^3 = 45$.

Figure 2: Scale space representation of a log-ratio image using three different reconstructions.

where $I_{SS}^{\hat{n}}$ is the nth reconstruction of the log-ratio image in the scale space constituted of N different reconstructions, $\|.\|_k$ denotes the l_k norm, D is the 2-D derivative operator, λ_1^n and λ_2^n are scalar parameters weighting the terms of the cost function for the nth reconstruction. Specifically, the first term of the cost function is the data fidelity term, the second and the third terms are for enhancing point based and region based features respectively. The relative magnitudes of weights help smooth out the image, thus resulting in homogeneous regions in terms of texture, while preserving edges and bright point reflectors. Fig. 2 shows a sample scale space representation with three different reconstructions of a log-ratio image. It can be observed from Fig. 2 that when the relative weight of λ_2 is increased, low contrast regions are gradually merged with their surrounding background completely losing their texture while high contrast regions are reconstructed with their contours smoothed.

2.3 Maximally Stable Extremal Region analysis of scale space images

Matas *et al.*[16] introduced an affinely-invariant stable local detector aimed to map correspondences between pair of images taken from different viewpoints. The rationale of obtaining extremal regions is to threshold a given amplitude image with all possible values within its dynamic range and to construct a hierarchical tree where nodes at each depth represent connected components. The analysis of each branch of the component tree yields maximally stable extremal regions where regions whose size remains approximately the same between consecutive nodes denoting parent and child are sought. To elaborate, a particular connected region Q_t obtained by thresholding the image at a value t is maximally stable, if

$$\Upsilon\left(Q_t\right) = \left|Q_{t+\triangle} \setminus Q_{t-\triangle}\right| / \left|Q_t\right| \tag{3}$$

attains a local minimum of the branch of interest where $|.|$ denotes the cardinality, $\setminus$ denotes the set difference, and $\triangle$ is the stability range parameter denoting the step size of threshold increments. Since the value of t satisfying the stability criterion can differ for each region, MSER analysis constructs each extremal region by thresholding a given image at a particular value, rather than a global threshold, to obtain the binary image. As the log-ratio image generally suffers from speckle noise, it is mostly impractical to use MSER analysis directly, so we propose to use MSER analysis on the reconstructions of the log-ratio image, namely scale space images, to obtain changed regions composing the change map. Within our context, on the one hand, as FPD achieves reconstructions with speckle noise reduction yielding homogeneous regions while not neglecting shape detail priors, changed regions having high contrast in the log-ratio image are easily detected as maximally stable extremal region candidates dissociating from background clutter. On the other hand, slightly changed regions having relatively lower contrast in the log-ratio image might merge with the background upon applying the FPD operator.

2.4 Change map generation through fusion

In order to mitigate the problem of not recovering relatively low contrast regions as maximally stable extremal regions and to circumvent the possible boundary extension of smoothed regions, we propose to combine the MSERs of scale space images within a fusion scheme. Having obtained MSERs of each scale space image, we introduce a feature-based fusion method, which we call *"selective scale fusion"* (SSF), where contrast and boundary curvature of each MSER are considered. The method is iterative starting MSER investigation at scale N and going down to the initial scale, and consists of the following seven stages:

1) Initialization: Let $X = [0,\, H[\cap \mathbb{N} \times [0,\, W[\cap \mathbb{N}$ be the domain on which the scale space images are defined and let $D_{CM} \subset X$ be the subset of the change map domain representing the set of changed pixels determined by our fusion algorithm. Adopting to map unchanged pixels to a binary value of 0 and changed pixels to a binary value of 1, our fusion algorithm is initialized by setting $I_{CM} : X \rightarrow 0$, and $D_{CM} = \emptyset$.

2) MSER sets construction: In order to be able to analyze MSERs found in all the scale space images and to extract features to be used in the decision of incorporating MSERs to the change map, connected component analysis is done:

$$S_k = \underset{j=1,\,...,\,M_k}{\{\cup R_{kj}\}}\ ,\ k = 1,\ ...,\ N \tag{4}$$

where k represents the scale index, j represents the connected region index, and S_k represents the MSER set of cardinality M_k constituted of connected regions R_{kj} obtained from the kth scale space image.

3) MSER association and classification: To carry out fusion of MSERs from scale space images, MSERs are further classified to be of intra-scale or inter-scale type. Intra-scale type MSERs are members of an MSER set of a single scale. Inter-scale type MSERs are members of MSER sets of more than one scale. This classification is done to identify whether an MSER is possibly originated from speckle noise for an intra-scale type and to provide a scale selection capability for a possibly changed region candidate for an inter-scale type. At the MSER investigation of ith scale space image and for the jth particular connected region R_{ij}, this classification is achieved by a simple association of the connected region between scales defined as follows:

$$c_k = \underset{j'=1,\,...,\,M_k}{argmax}\, |R_{ij} \cap \{\cup R_{kj'}\}|,\ k = 1,\ ...,\ i \tag{5}$$

where all the connected regions composing the MSER set of scale space images starting from the initial scale to the scale being analyzed are investigated. The corresponding connected region index c_k from the kth scale space image having maximum intersection with the connected region R_{ij} is kept. The classification of the MSER is then defined as follows:

$$R_{ij} \in \begin{cases} inter\text{-}scale\, MSER, & \text{if } \exists k \in \{1,\ ...,\ i-1\} : |R_{kc_k} \cap R_{ij}| \,/\, |R_{ij}| \geq \Gamma_{\texttt{region}} \\ intra\text{-}scale\, MSER, & \text{otherwise} \end{cases} \tag{6}$$

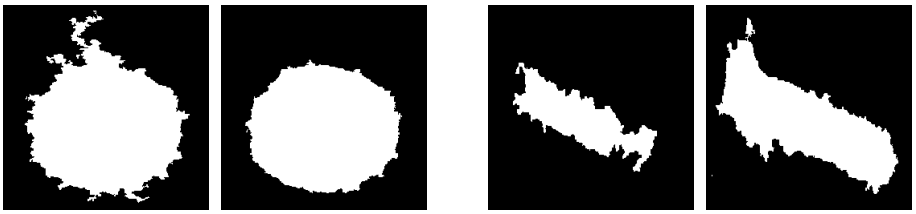

(a) A connected region obtained from 1st scale space image(left), and 2nd scale space image(right).

(b) A connected region obtained from 1st scale space image(left), and 2nd scale space image(right).

Figure 3: Connected regions exemplifying (a) inter-scale and (b) intra-scale type MSERs.

which requires a certain amount of intersection achieved between connected regions to be considered as an inter-scale MSER controlled by a threshold of value $\Gamma_{\texttt{region}}$. Fig. 3 demonstrates a particular example of inter-scale type and intra-scale type MSERs involving two scale space images. In Fig. 3a the MSER in the 2nd scale space image is classified as inter-scale type since the intersection threshold is exceeded between regions, whereas the MSER in the 2nd scale space image in Fig. 3b is classified as intra-scale type since the minimum intersection criterion is not satisfied.

4) Feature extraction: After the type of the MSER region, R_{ij}, is determined, contrast and boundary curvature features from the associated connected regions and the region being analyzed are extracted. A feature metric combining contrast and boundary curvature is formed. The feature metric favors connected regions having smooth boundaries with the curvature term and avoids selecting the connected regions whose boundaries are extended during the scale space construction with the contrast term. The feature metric of the associated connected regions is calculated as:

$$f_k = \begin{cases} \alpha cur\left\{R_{kc_k}\right\} + (1-\alpha)\, cont\left\{R_{kc_k}\right\}, & \text{if } \left|R_{kc_k} \cap R_{ij}\right| / \left|R_{ij}\right| \geq \Gamma_{\texttt{region}} \\ 0, & \text{otherwise} \end{cases}, \; k = 1, \ldots, i \tag{7}$$

where $cur\left\{.\right\} \in [0,1] \cap \mathbb{R}$, $cont\left\{.\right\} \in [0,1] \cap \mathbb{R}$ denote the curvature and contrast operators, and $\alpha \in [0,1] \cap \mathbb{R}$ is the feature blending parameter used to weigh the contribution of the curvature and contrast features. The curvature operator can be implemented using any algorithm such as the k-cosine curvature algorithm[18], and the contrast operator can be implemented by applying morphological operators.

5) Incorporation of MSER to the change map: The scale member having the best feature metric for an inter-scale type MSER, and an intra-scale type MSER whose feature metric is above a threshold is added to the change map. With this strategy, scale selection capability for an inter-scale type MSER is introduced jointly evaluating the associated connected regions. Meanwhile, intra-scale type MSERs not bearing sufficient feature metric and thus possibly originating from speckle noise are eliminated. The scale selection and the update of the change map domain are obtained as:

$$b = \underset{k=1,\ldots,i}{argmax} f_k \tag{8}$$

$$D_{CM} = \begin{cases} D_{CM} \cup R_{bc_b}, & \text{if } R_{ij} \in \textit{inter-scale}\, MSER \\ D_{CM} \cup R_{ij}, & \text{if } R_{ij} \in \textit{intra-scale}\, MSER \wedge\ f_i \geq \Gamma_{\texttt{feature}} \end{cases} \tag{9}$$

where b represents the scale index having best feature metric among all the associated regions, and $\Gamma_{\texttt{feature}}$ is the feature metric threshold value for an intra-scale type MSER to be considered as a changed region.

6) MSER sets reduction: As a concluding step of the analysis of a particular inter-scale type MSER, associated connected regions of the unselected scales are masked for the succeeding iteration to avoid duplicate investigation since a connected region having best feature metric is already added to the change map. For an intra-scale type

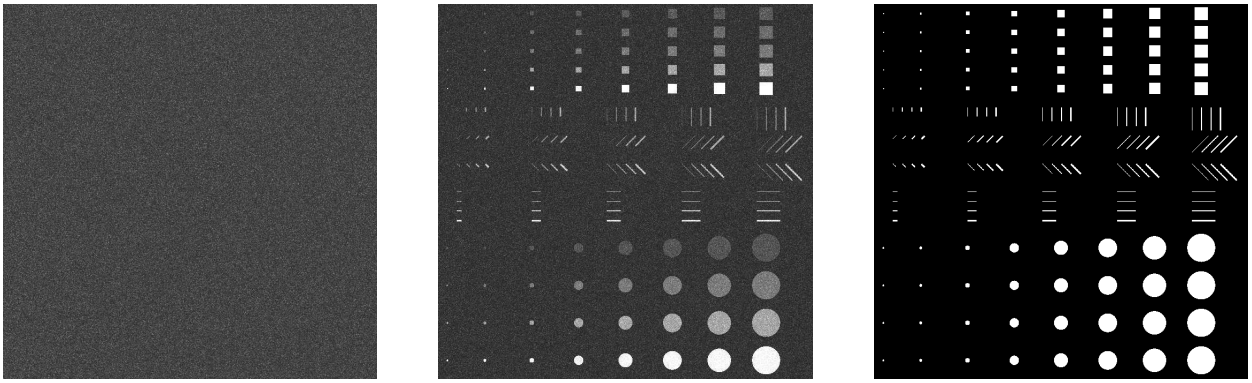

(a) I_{t_1} sea clutter image. (b) I_{t_2} sea clutter image with synthetic change. (c) Ground truth image.

Figure 4: First data set consisting of multitemporal images and the ground truth change map.

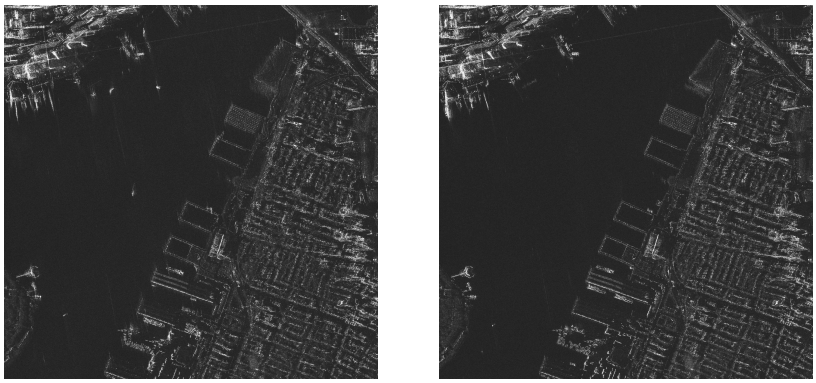

(a) I_{t_1} seaport image acquired on October 20, 2011. (b) I_{t_2} seaport image acquired on December 25, 2011.

Figure 5: Multitemporal seaport images of New York acquired on October 20, 2011 and December 25, 2011.

MSER this step is irrelevant since no such association is present between MSER sets of scale space images. The masking is simply achieved as follows:

$$S_k = \begin{cases} S_k \setminus R_{kc_k}, & \text{if } R_{kc_k} \neq \emptyset \wedge R_{ij} \in \textit{inter-scale}\, MSER \\ S_k, & \text{otherwise} \end{cases}, k = 1, ..., i. \tag{10}$$

7) Change map generation: After all the MSERs of all scale space images are investigated by repeating steps 3-6, the change map is generated by mapping the domain D_{CM} to a binary value of 1, i.e.,

$$I_{CM} : D_{CM} \rightarrow 1. \tag{11}$$

3. EXPERIMENTAL RESULTS

3.1 Data sets

In order to assess the performance of our proposed change detection algorithm, two different data sets are used to conduct the experiments. The first data set is comprised of multitemporal images in which changes are generated synthetically, whereas the second data set is comprised of real multitemporal images. These data sets are formed

from images of New York City acquired by the TerraSAR-X satellite on October 20, 2011 and December 25, 2011 in spotlight single polarization mode and of size 19000×20000 pixels.

The first data set is comprised of two different sea clutter image patches. The images are of 4000×4000 pixels with a spatial resolution of 1 m. A synthetic change image constituted of different shapes with several orientations, sizes, and backscatter amplitude levels representing a variety of possible changes is superimposed on one of the image patches to form the first set of multitemporal images. These synthetic changes almost constitute 10% of the area of the observed scene. Fig. 4 shows this first data set along with the ground truth map of the synthetic change image.

The scene of interest in the second data set is a seaport. These images are also of 4000×4000 pixels in size with a spatial resolution of 1 m where no ground truth map is available. The second set of multitemporal images are depicted in Fig 5.

3.2 Quantitative measures

To quantitatively evaluate the performance of our change detection algorithm on the first data set in the following subsections, we revisit some of the popular metrics used. Letting I_{GT} and D_{GT} be the ground truth image and the domain of changed regions respectively, i.e., $I_{GT} : \{D_{GT} \subset X\} \rightarrow 1$, the metrics are defined as follows:

Jaccard Index is a type of a metric used to measure the similarity and diversity between sample sets, defined to be:

$$J(D_{GT},\, D_{CM}) = \frac{|D_{GT} \cap D_{CM}|}{|D_{GT} \cup D_{CM}|} \tag{12}$$

The Jaccard index penalizes false detections to the extent it rewards true detections making it a widely used performance evaluator.

Precision reveals the rate of true detections among all the detections, i.e.,

$$Precision = \frac{|D_{GT} \cap D_{CM}|}{|D_{CM}|} \tag{13}$$

Recall measures the rate of true detections among all the changed regions, i.e.,

$$Recall = \frac{|D_{GT} \cap D_{CM}|}{|D_{GT}|} \tag{14}$$

3.3 Effect of scale space size

One of the most critical impacts on algorithm performance is the size of the scale space, namely the number of log-ratio image reconstructions composing the scale space images. In order to demonstrate that the information provided from each scale space image is additive irrespective of a detailed analysis and selection of reconstruction parameters for a given scale space size, we propose to setup an experiment on the first data set introduced in subsection 3.1 by linearly sampling the interval of predefined parameters used to generate reconstructions. After an empirical analysis of the effect of parameter selections, we decided to use the following set of parameters and thresholds for scale space generation and MSER fusion:

$$\lambda_1^{n \in [1,N] \cap \mathbb{N}} = 0,\ \lambda_2^1 = 15,\ \lambda_2^N = 47$$

$$\Gamma_{\texttt{region}} = 0.8,\ \Gamma_{\texttt{feature}} = 0.7,\ \alpha = 0.5$$

Quantitative results of the effect of scale space size analysis are tabulated in Table 1. The change detection algorithm and the experiments are realized in C++ using OpenCV 2.4 API with a workstation of an Intel i7 3.06 GHz CPU with 4 cores and 8 hardware thread support where specifically NVidia GTX 560 TI 1.65

Table 1: Jaccard index, precision, and recall performance values of the proposed change detection algorithm applied on first data set along with execution times for various scale space sizes.

N	Jaccard Index	Precision	Recall	Total execution time in seconds
2	0.742	0.987	0.749	10.511
3	0.758	0.986	0.766	14.225
4	0.825	0.981	0.838	18.348
5	0.882	0.987	0.892	22.408
6	0.896	0.987	0.907	27.015
7	0.938	0.983	0.953	30.385
8	0.938	0.981	0.956	35.004
9	0.943	0.987	0.955	40.464
10	0.936	0.984	0.950	44.582
11	0.956	0.987	0.968	48.872
12	0.959	0.987	0.971	53.365

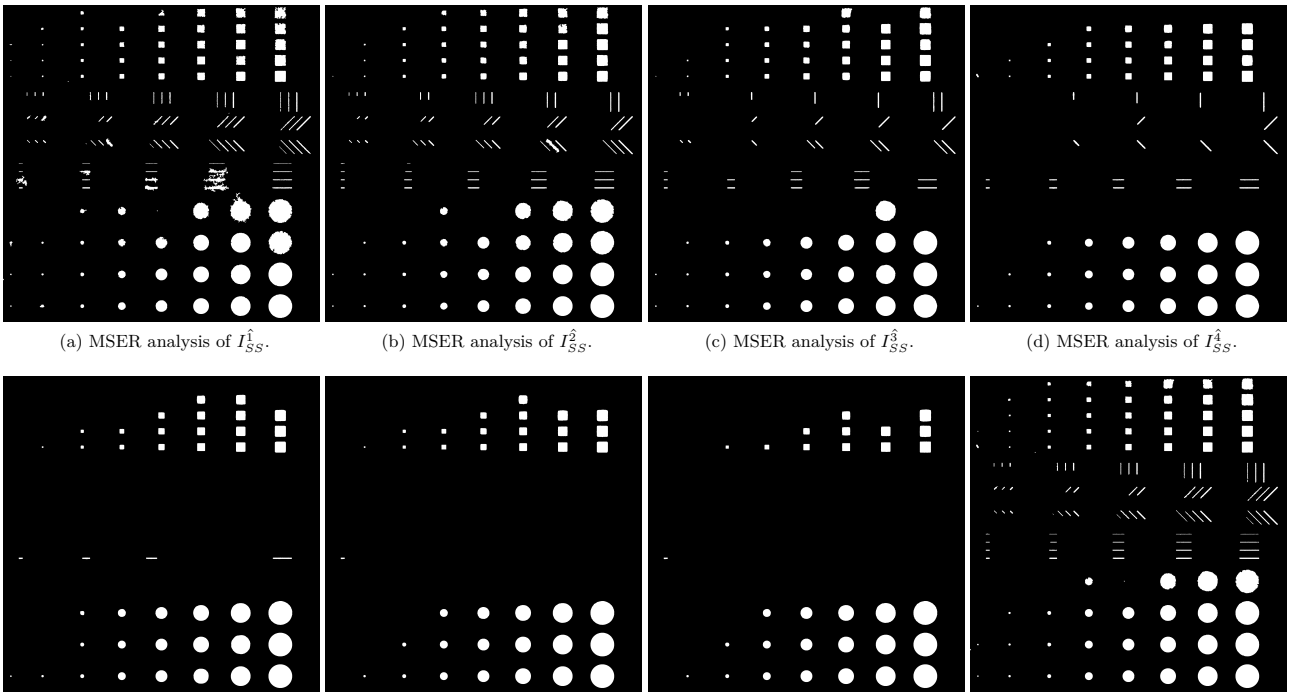

(a) MSER analysis of $I^{\hat{1}}_{SS}$. (b) MSER analysis of $I^{\hat{2}}_{SS}$. (c) MSER analysis of $I^{\hat{3}}_{SS}$. (d) MSER analysis of $I^{\hat{4}}_{SS}$.

(e) MSER analysis of $I^{\hat{5}}_{SS}$. (f) MSER analysis of $I^{\hat{6}}_{SS}$. (g) MSER analysis of $I^{\hat{7}}_{SS}$. (h) Change map result.

Figure 6: Qualitative results obtained on the first data set.

GHz GPU with 384 cores is utilized to implement the FPD operator. From the acquired results, the total execution time of the algorithm seems to scale linearly with the scale space size. Besides, as can be seen from the performance metrics, the increase in scale space size results in improved values of recall signifying the additive change information provided from each scale space image, whereas among all the detections almost the same precision values are achieved supporting the robustness and efficiency of our proposed fusion scheme. The performance of the algorithm saturates when scale space size is further increased which is not shown Table 1. The small fluctuations in the performance metrics when scale space size increases are due to the linear sampling of parameters where each time not same set of previously reconstructed images form the scale space when an additional scale space image is to be generated.

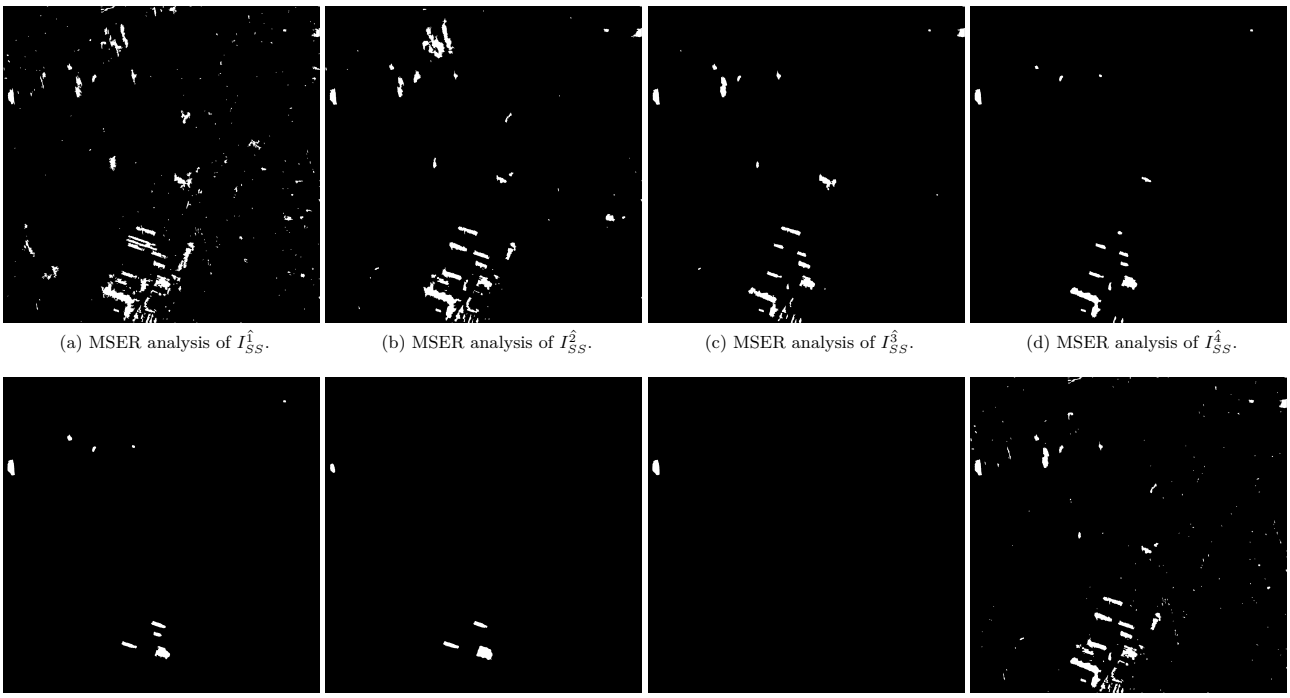

(a) MSER analysis of $I_{SS}^{\hat{1}}$. (b) MSER analysis of $I_{SS}^{\hat{2}}$. (c) MSER analysis of $I_{SS}^{\hat{3}}$. (d) MSER analysis of $I_{SS}^{\hat{4}}$.

(e) MSER analysis of $I_{SS}^{\hat{5}}$. (f) MSER analysis of $I_{SS}^{\hat{6}}$. (g) MSER analysis of $I_{SS}^{\hat{7}}$. (h) Change map result.

Figure 7: Qualitative results obtained on the second data set.

(a) I_{t_1} seaport image acquired on October 20, 2011.

(b) I_{t_2} seaport image acquired on December 25, 2011.

(c) I_{t_2} seaport image acquired on December 25, 2011 with changes marked in color.

Figure 8: Qualitative results obtained on the second data set demonstrating the objects that have probably entered/departed the scene of interest.

3.4 Change detection analysis on data sets

Based on the results obtained for the first data set which are shown in Table 1, the use of seven scale space images results in good overall performance whilst detecting changes in a fairly changed scene of interest in half a minute reaching a moderate compromise between computation time and algorithm performance. Using the same set of parameters to generate scale space representation and MSER fusion we exhibit our qualitative results obtained on the data sets in Fig. 6 and Fig. 7. Due to the different reconstructions achieved in scale space images, various different connected component tree representations are realized during MSER analysis. This eventually leads to different MSERs found from scale space images. Fig. 6 and Fig. 7 visually demonstrate the fact that no complete subset-superset relation holds in between MSER sets of scale space images supporting the idea that each scale space image can provide different information. In order to present a visually more pleasing qualitative result of the change map obtained using the second data set, objects that have probably departed the scene between image acquisiton times are marked in green color whereas objects that have probably entered the scene are marked in red color and depicted in Fig. 8. The encolouring is based on the mean backscatter amplitude change analysis of regions composing the change map.

4. CONCLUSION

In this paper, an unsupervised change detection method for SAR imagery is proposed based on MSER analysis of scale space images. The scale space images achieving various levels of speckle noise reduction and shape detail preservation in reconstructing the log-ratio image are formed using the FPD operator. On the one hand, since this is a segmentation based approach, highly changed regions with a high contrast signature in the log-ratio image easily pass as MSER candidates and formed with accurate boundaries with the help of speckle reduction achieved by virtue of the FPD operator. On the other hand, slightly changed regions with a low contrast signature in the log-ratio image might suffer from a complete texture loss and merge with the background during the scale space construction, which necessitates a fusion algorithm studying MSER analysis of each scale space image. Our proposed fusion algorithm, SSF, investigates intra/inter-scale MSERs and constructs the change map composed of MSERs selected by a feature metric combining curvature and contrast measures which mitigates the problem of not recovering slightly changed regions, as well as eliminates regions possibly originating from speckle noise. The qualitative and quantitative results demonstrate that the proposed fusion method works effectively in constructing the boundaries of changed regions achieving high precision.

Within the context of our proposed change detection algorithm, it has been demonstrated that the information provided by each scale space image is additive hence resulting in higher change detection performance when the scale space size, which is a parameter to be selected, is increased. An important issue is the automatic selection of reconstruction parameters to obtain the scale space representation for a predetermined number of scale space size, which is a topic worth studying in future work.

REFERENCES

[1] Inglada, J., and Mercier, G., "A new statistical similarity measure for change detection in multitemporal SAR images and its extension to multiscale change analysis," *IEEE Trans. Geosci. Remote Sens.* **45**(5), 1432-1445 (2007).

[2] Radke, R. J., Andra, S., Al-Kofahi, O., and Roysam, B., "Image change detection algorithms: A systematic survey," *IEEE Trans. Image Process.* **14**(3), 294-307 (2005).

[3] Mercier, G., and Derrode, S., "SAR image change detection using distance between distributions of classes," in [*IEEE International Geoscience and Remote Sensing Symposium (IGARSS)*], **6**, 3872-3875 (2004).

[4] Bazi, Y., Bruzzone, L., and Melgani, F., "An unsupervised approach based on the generalized Gaussian model to automatic change detection in multitemporal SAR images," *IEEE Trans. Geosci. Remote Sens.* **43**(4), 874-887 (2005).

[5] Moser, G., and Serpico, S. B., "Generalized minimum-error thresholding for unsupervised change detection from SAR amplitude imagery," *IEEE Trans. Geosci. Remote Sens.* **44**(10), 2972-2982 (2006).

[6] El-Darymli, K., McGuire, P., Power, D., and Moloney, C., "Target detection in synthetic aperture radar imagery: a state-of-the-art survey," *Journal of Applied Remote Sensing* **7**(1), (2013).

[7] Huang, S. Q., Liu, D. Z., and Cai, X. H., "A new change detection algorithm for SAR images," in [*Asian-Pacific Conference on Synthetic Aperture Radar (APSAR)*], 729-732 (2009).

[8] Zhang, X., Chen, J., and Meng, H., "A novel SAR image change detection based on Graph-Cut and generalized Gaussian model," *IEEE Geosci. Remote Sens. Lett.* **10**(1), 14-18 (2013).

[9] Celik, T., and Yetgin, Z., "Change detection without difference image computation based on multiobjective cost function optimization," *Turk. J. of Elec. Eng. & Comp. Sci.* **19**(6), 941-956 (2011).

[10] Yetgin, Z., "Unsupervised change detection of satellite images using local gradual descent," *IEEE Trans. Geosci. Remote Sens.* **50**(5), 1919-1929 (2012).

[11] Moser, G., and Serpico, S. B., "Unsupervised change detection from multichannel SAR data by Markovian data fusion," *IEEE Trans. Geosci. Remote Sens.* **47**(7), 2114-2128 (2009).

[12] Bovolo, F., and Bruzzone, L., "A detail-preserving scale-driven approach to change detection in multitemporal SAR images," *IEEE Trans. Geosci. Remote Sens.* **43**(12), 2963-2972 (2005).

[13] Bazi, Y., and Melgani, F., "A variational level-set method for unsupervised change detection in remote sensing images," in [*IEEE International Geoscience and Remote Sensing Symposium (IGARSS)*], **2**, 984-987 (2009).

[14] Celik, T., "Multiscale change detection in multitemporal satellite images," *IEEE Geosci. Remote Sens. Lett.* **6**(4), 820-824 (2009).

[15] Celik, T., and Ma, K. K., "Multitemporal image change detection using undecimated discrete wavelet transform and active contours," *IEEE Trans. Geosci. Remote Sens.* **49**(2), 706-716 (2011).

[16] Matas, J., Chum, O., Urban M., and Pajdla T., "Robust wide baseline stereo from maximally stable extremal regions," in [*Proc. of British Machine Vision Conference (BMVC)*], 384-396 (2002).

[17] Cetin, M., and Karl, W. C., "Feature-enhanced synthetic aperture radar image formation based on non-quadratic regularization," *IEEE Trans. Image Processing* **10**(4), 623-631 (2001).

[18] Sun, T. H., Lo, C. C., Yu, P. S., and Tien, F. C., "Boundary-based corner detection using K-cosine," in [*Proc. of IEEE International Conf. on Systems, Man and Cybernetics*], 1106-1111 (2007).